Ground ice content of the frozen active layer and near-surface permafrost in the Rankin Inlet area, Nunavut, Canada

Benoit Faucher[1], Anne-Marie LeBlanc[1], Greg A. Oldenborger[1], Emmanuel Carrière[2], Denis Lacelle[2] & Philippe Letellier[3]

[1]*Geological Survey of Canada, Natural Resources Canada, Ottawa, Ontario, Canada*

[2]*Department of Geography, Environment and Geomatics, University of Ottawa, Ottawa, Ontario, Canada*

[3]*Institut National de Recherche Scientifique, Québec City, Québec, Canada*

Abstract

In the context of climate change, the distribution and amount of ground ice in permafrost is critical to evaluate surface disturbances and geohazard risks. Ground ice conditions are poorly defined in northwestern Hudson Bay in the central Canadian Arctic, an area with renewed development interest. Here, we report on the near-surface (< 2 m) ground ice content of the frozen active layer and permafrost from three sites with different surface materials near Rankin Inlet, Nunavut. Cores were retrieved from nearshore, till, and alluvial deposits (all intermixed with marine sediments). Ground ice content derived from CT scan images and laboratory measurements suggested a relatively high abundance of ground ice in the nearshore marine sediments and alluvial/marine sediment cores with a lower overall content in the till/marine sediment core. Computed tomography scan analyses commonly underestimated volumetric ice content compared to laboratory measurements. This may have been caused by the coarse pixel resolution of our CT scan images (0.6 mm), making the pore space diameters of our sampled fine sediments partially unresolvable. Further, in situ seasonal thaw settlement measurements taken at each site from heave sleeves corroborated our laboratory-derived excess ice content measurements reasonably well. Excess ice content measurements were also used to predict active layer thickness increases and ground subsidence under future air temperature increases. Overall, our study provides new information on ground ice conditions in the Rankin Inlet area of Nunavut.

1 Introduction

Accurate knowledge of the distribution and amount of ground ice in permafrost is critical to evaluating ground surface (GS) disturbances and geohazard risks in Arctic regions destined for development. It is generally accepted that permafrost-bearing soils' total annual GS subsidence (GSS) should depend on 1) thaw settlement, controlled by ground ice content; and 2) volume-compressibility caused by surcharge load and self-weight (Watson et al. 1973). The latter is often disregarded because consolidation comprises only a fraction of the surface settlement (Taber 1930). In addition, the thaw settlement potential of heterogeneous soils can often be assessed by determining the edaphic properties (e.g., dry densities of soils in frozen and thawed states) of individual soil horizons with depth. This permits the calculation of their thaw strain (Pullman et al. 2007; Crory 1973). However, thaw strain can also be derived from excess ice content (EIC) measurements (i.e., van Everdingen 2005) converted into a volumetric ratio of cumulative EIC to the total thickness of the thawed soil column (Castagner et al. 2022). These data are often indispensable to predicting local GSS and possible infrastructure damage (Doré et al. 2016).

Information on ground ice content, particularly EIC, is available from northwest Canada and a few sites in the eastern Arctic but is otherwise limited. There is little information on ground ice from the northwestern Hudson Bay area around Rankin Inlet, where the air temperature is increasing, and significant infrastructure development is occurring (LeBlanc and Oldenborger 2021).

Recent research has documented the thermal state of permafrost (Oldenborger et al. 2017; LeBlanc and Oldenborger 2021) and approximated seasonal GSS (Leblanc et al. 2019; Oldenborger et al. 2020) in the vicinity of Rankin Inlet. However, due to the scarcity of sampled and investigated permafrost cores, empirical volumetric ice content (VIC) and EIC measurements remain almost nonexistent (McCuaig et al. 2022).

This study investigates the VIC and EIC of the near-surface (< 2 m) permafrost (which includes the frozen active layer) at study sites near Rankin Inlet. The goals of this study are to 1) document and describe ground ice content in sampled soil units using laboratory measurements and to compare those with computed tomography (CT) scan measurements; and 2) assess site-specific GSS potential of our investigated frozen active layer/permafrost sampling sites under climate warming-induced thaw penetration (TP) increases. Overall, our study provides new information for understanding ground ice content and spatial distribution within the Rankin Inlet area of Nunavut.

2 Study Area

The hamlet of Rankin Inlet is in the Kivalliq region of Nunavut (Canada) on the western coast of Hudson Bay (Figure 1). The hamlet's territory is within the western Churchill Province of the Canadian Shield. Its complex geology consists of Archaean Rankin Inlet Greenstone Belt felsic volcanic rocks intercalated with mafic volcanic and sedimentary rocks and granodioritic to tonalitic intrusions (Lawley et al. 2016). The surficial geology consists of

https://doi.org/10.52381/ICOP2024.80.1

glacial, marine, and glaciofluvial deposits, including eskers, with numerous bedrock outcrops (McMartin 2002) that shape the topography with elevation ranging from sea level to 300 m. The Laurentide Ice Sheet covered the region during the Wisconsin glaciation and receded by ~6 kyr BP (Dyke 2004). The postglacial Tyrrell Sea extended up to 150 km inland from the current coastline over the isostatically depressed land surface, reaching a maximum elevation of approximately 170 m above the present sea level; (Dyke 2004; Randour et al. 2016; McMartin et al. 2023).

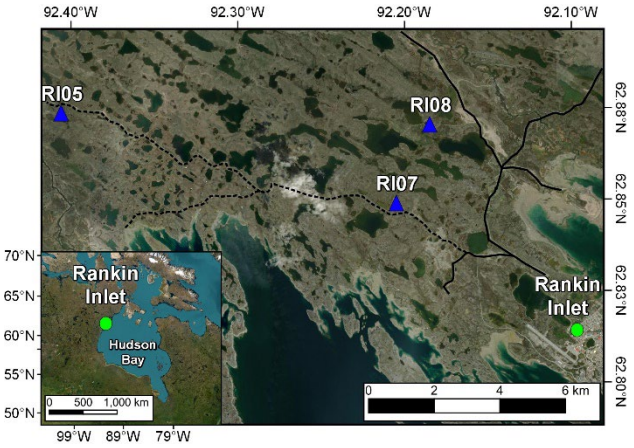

Figure 1. Location map of the frozen active layer/permafrost coring sites near Rankin Inlet (Nunavut). Coring sites and Rankin Inlet hamlet are indicated with blue triangles and green circles, respectively. Continuous and dotted lines show main roads and access trails. The background is a 0.46 m MAXAR Vivid image (September 3rd, 2022) of the area of interest.

The mean annual air temperature (MAAT) for Rankin Inlet was -10.3 °C from 1981–2020 (Environment and Climate Change Canada 2022), with an average increase of 0.05 ± 0.02 °C/year. Over the same period, the average total precipitation was 315 mm, with rainfall accounting for 184 mm and snow precipitations contributing 131 cm. There was no significant trend in total precipitation from 1981 to 2020.

Rankin Inlet is within the continuous permafrost zone, and the base of permafrost was estimated between 285 m and 430 m, with thinner permafrost being near lakes (Golder 2021). The geothermal gradient varies between 0.01 and 0.02 °C/m (Golder 2014), while the mean annual ground temperature at the top of permafrost ranges between -9.5 and -5.5 °C (LeBlanc and Oldenborger 2021). Active-layer thickness ranges from ~0.5 m in organic-rich alluvial/marine sediments to ~1.6 m in marine and organic-poor till deposits (LeBlanc and Oldenborger 2021).

3 METHODOLOGY

3.1 Field sampling

Study sites for ground temperature boreholes and permafrost coring in the Rankin Inlet region were planned to represent various terrain conditions, including developed and undeveloped land and different geological settings. Site locations were established after considering surficial geology, land access, community consultation, and field observations. Data from three shallow borehole sites with different surficial geology are analyzed herein: nearshore marine sediments (RI05); till and marine sediments (RI07); and alluvial and marine sediments (RI08; Figure 1). Site details and field observations concerning the retrieved cores and their sediments/apparent cryostructures are given by LeBlanc and Oldenborger (2021).

Boreholes at sites RI05 and RI07 were drilled in June 2018 and 2019 at site RI08 using a portable earth drill using barrels with diamond core bits modified from Calmels et al. (2005). Any unfrozen organic mat and unfrozen sediments to a depth of 2 to 15 cm were removed, set aside, and replaced as best as possible to reduce thermal disturbances as much as possible. However, some thermal disturbance to the sites occurred. Cores were measured and visually logged during drilling, bagged in plastic, and frozen for further analysis.

The shallow boreholes were cased with either sealed 1 ½" PVC pipe with an internal multi-core thermistor cable in silicone bath oil (RI05 and RI07) or with open ¾" PVC pipe with individual external thermistors (RI08). Thermistors were routed to the surface and logged continuously with 4-hour recording intervals. Ground temperatures were recorded with RBR data loggers (0.01 °C resolution; RI05 and RI07) and an Onset HOBO U12 data logger (± 0.25 °C accuracy; RI08). Ground surface temperatures (2–5 cm depth) were recorded with 4-hour recording intervals with Onset HOBO Water Temp Pro v2 loggers (± 0.21 °C accuracy; all sites).

3.2 Computed tomography scanning and image processing

For the last two decades, computed tomography (CT) scans have routinely been used to rapidly quantify volumetric ground ice contents and produce high-resolution cryostratigraphic profiles of permafrost-bearing soils (e.g., Calmels and Allard 2004, 2008; Gadylyaev et al. 2021; Fan et al. 2021).

For our study, the samples were scanned at the Institut national de la recherche scientifique (INRS) using a SOMATOM Definition AS+ 128 CT scanner by SIEMENS at 140 kV and with an exposure of 200 mAs. We then segmented the CT scan images of our permafrost cores to obtain a quick first-order estimate of their VIC and/or EIC. This was done by applying a non-local means filter to the volume to help with thresholding. The volume was then segmented (based on the visual inspection of the cores' CT scan images) using four different thresholds: air (-1024 to -500 HU), ice (-500 to 700 HU), sediment (700 to 1500 HU) and rock (1500 HU or more). For some volumes, morphological operations like opening and hole filling were applied. The segmented volumes are then recombined into a single volume, with each material having a different value. A statistical analysis was finally run on the combined volume to determine on each CT slice the percentage of the sample's area covered by each material.

3.3 Laboratory ground ice content measurements

The three frozen active layer/permafrost cores were sliced at ~2 cm intervals using a diamond blade-equipped tile saw. The frozen slices were left to thaw in sealed plastic bags and then transferred into 250 ml High-Density Polyethylene (HDPE) tubes.

EIC for each ~2 cm segment was derived from supernatant water measurements and was derived (based on Kokelj and Burn 2003) using:

$$\mathrm{EIC}(\%) = \frac{\mathrm{Ws}*1.0917}{(\mathrm{Ws}*1.0917+\mathrm{Vs})} * 100 \quad [1]$$

where *Ws* is the volume of supernatant water (cm^3), *Vs* is the volume of sediments (cm^3), and the number 1.0917 is used to convert the measured volume of supernatant water to the equivalent ice volume (Lapalme et al. 2017).

VIC was calculated (from French 2017) using:

$$\mathrm{VIC}(\%) = \frac{\mathrm{Wv}*1.0917}{\mathrm{Vt}} * 100 \quad [2]$$

where Wv is the volume of the water in the sample (cm^3), and Vt is the total volume of the sample (cm^3) established from the core dimensional data. The total mass of water in the sample (g) is used to derive Wv, assuming a water density of 1.0 g cm^3.

The measurement precision was within 1 ml; this translates to ± 1% errors in reported values. Missing data points (e.g., instances where a core segment was missing for a particular depth) were filled by deriving the mean of surrounding values. The same data-infilling approach was used to estimate the ground ice content at each site at a 1 cm resolution to approximate current and future GSS at our three sites.

A linear regression analysis (including derivations of adjusted R2 values) in the R software (R core team 2023) was used to compare CT scan-derived vs. laboratory-derived VIC and EIC measurements.

3.4 Ground surface subsidence and thaw penetration measurements

The thaw penetration depth at each of our three field sites during the 2018 (RI05 and RI07) and 2019 (RI08) summers was estimated by linear interpolation of the temperature profile close to 0 °C and/or by linear extrapolation from sensors located on the unfrozen side of the 0 °C isotherm (Riseborough 2008). The accuracy of interpolation and extrapolation is approximately 0.05 and 0.1 m for thermistor spacings of 0.25 and 0.5 m, respectively (Riseborough 2008). Summer site-specific observed GSS was measured using timelapse cameras pointing towards graduated heave sleeves described in LeBlanc and Oldenborger (2021).

The laboratory-derived measurements of EIC in our three frozen active layer/permafrost cores were employed to simulate GSS and active layer thickness (ALT) variations under current and future seasonal TP increases. ALT increases related to TP augmentations were subsequently determined by subtracting predicted GSS from TP increases (e.g., for a 50 cm TP increase and a 20 cm GSS, the ALT increase is 30 cm).

4 RESULTS

4.1 Ground ice content

4.1.1 Nearshore marine sediment core (RI05)

Laboratory analyses of the RI05 core revealed two ice-rich sections with depth (Figure 2A). The first was at the top of the core (i.e., within a ~12 cm organic-rich section), with VIC reaching a maximum of 80% and EIC being nil. Below, between 12 and 100 cm (permafrost table), a layer of silty sand sediments comprising localized gravel/pebble clasts and seashell fragments was encountered. VIC remained relatively stable within this core section, and EIC remained at or near 0% to a depth of ~92 cm, where field observations suggested a transition to finer sediments (i.e., fine sands and silts, with the latter being more abundant), until progressively increasing to 72% at the permafrost table. The second ice-rich section was found below the permafrost table. From this depth to our maximum core retrieval depth of 144 cm, VIC and EIC ranged from 48 to 92% and 20 to 85%, respectively. We estimate that the average EIC in the upper 50 cm of the permafrost at the RI05 site was ~60%.

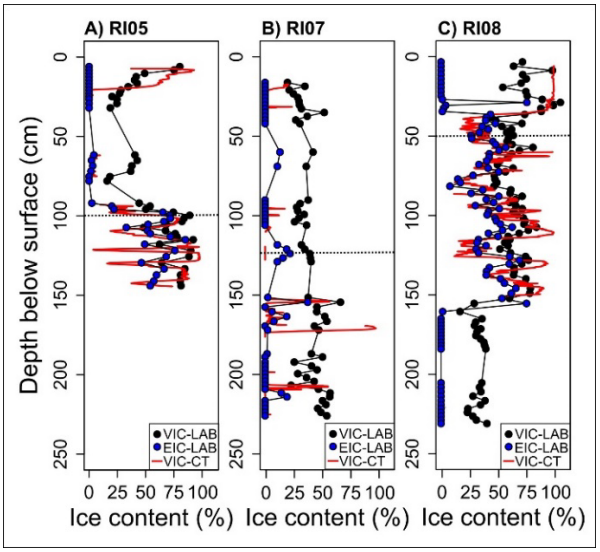

Figure 2. Laboratory (Lab) and computed tomography (CT) volumetric and excess ice contents (VIC; EIC) in the three frozen active layer/permafrost cores of the RI05 (panel A), RI07 (panel B) and RI08 (panel C) sites. The permafrost table depth relative to frozen conditions at each site is indicated with dashed lines.

4.1.2 *Till and marine sediment core (RI07)*

The RI07 core exhibited the most homogeneous ground ice content with depth out of all three sampled surficial deposit units (Figure 2B). The core was characterized by a ~4 cm thick layer of organics under which sandy sediments were observed to a depth of ~30 cm. The 30–175 cm core section is occupied by sandy sediments with pebbles (with the occasional presence of finer grains) and seashells. Gray fine sediments (likely a mix of clays and silts) were observed from this depth until the bottom of the core (225 cm). No clear trend was noted with depth for VIC: it varied from 20 to 67%, and the most notable fluctuations were observed near the core bottom (~230 cm). The core contained EIC at three depth ranges. The first was encountered between 60 and 69 cm (our only two measurements in this depth range due to no core recovery or core discarded (too small) for analyses), where EIC averaged ~12%. In the second EIC-rich section, between depths of 121 and 187 cm, EIC ranged from 2 to 38%. The third EIC-rich section was at a depth of ~210 cm (average EIC% of ~17%), where ~0.5–1 cm ice lenses were encountered. We approximate the EIC in the upper 50 and 100 cm of the permafrost at the RI07 site to average ~13 and ~7%, respectively.

4.1.3 *Alluvial and marine sediment core (RI08)*

The RI08 site had the thickest (~40 cm) layer of organic matter (peat) out of all three sites. Below that, a layer of fine sediments and sand was present to a depth of ~165 cm. Sand intermixed with finer sediments were also present from this depth until the bottom of the core (230 cm), but unlike the overlying sediments, those were highly abundant in seashells. Two distinct VIC zones characterize the RI08 core (Figure 2C). The first VIC zone includes the upper ~150 cm of the core, where VIC averaged 67%. The most ice-rich sample retrieved from this core (a frost blister horizon of ~5–7 cm) was situated within this unit at ~28 cm depth within the organic layer: it had a VIC of 100%. VIC then became much lower and stable below 150 cm, averaging 23% to a depth of 230 cm. The EIC in the upper organic-rich section of the core (upper ~38 cm) was (or very close to) nil except for the frost-blister horizon, where EIC was measured at 76%. Below that, the remaining 8 cm peat horizon had an average EIC of ~13%. A slight progressive increase in EIC was then noted from 38 to 155 cm, below which (to our maximum sampling depth of 230 cm) EIC was zero. We approximate the EIC in the upper 50 and 100 cm of the permafrost at the RI08 site to average ~38 and ~44%, respectively.

4.2 Ground surface subsidence during the 2018 and 2019 summers

GSS measurements from heave sleeve photographs at the RI05, RI07 (2018 summer) and RI08 (2019 summer) sites reached a maximum of 6.8, 4.5, and 12 cm, respectively (Figure 3). Those observations agreed reasonably well with the total predicted EIC-based GSS under interpolated TP at each site in 2018 or 2019 (RI05 = 5.8 cm; RI07 = 4.7 cm; RI08 = 15.1 cm). Additionally, the temporal evolution of observed GSS matched the EIC-based GSS predictions over the 2018 summer for the RI05 and RI07 sites. Still, by comparison, predicted GSS lags observations during the 2018 summer. Conversely, at the alluvial and marine sediment (RI08) site, the observed GSS lagged considerably behind predicted GSS during the 2019 summer TP.

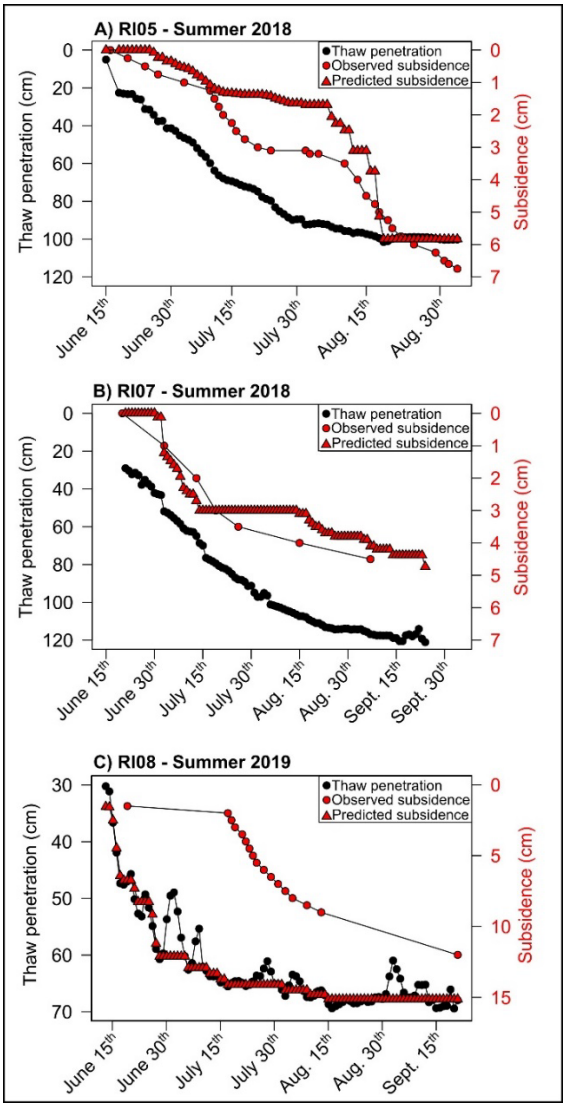

Figure 3. Time series of interpolated TP (black dots; for initial frozen conditions before GSS), observed (red dots) and predicted (red triangles) GSS during the 2018 (RI05 and RI07) and 2019 (RI08) summers. TP interpolations begin at 40 cm and 30 cm for the RI07 and RI08, respectively, since thermistor cables were only installed at those sites in mid-June. TP had already begun, and an initial ~1.5 cm of GSS had been observed (on the existing heave sleeve) beforehand at the RI08 site.

4.3 Predicted active layer dynamics and ground surface subsidence under climate warming

Our upper permafrost degradation simulations (i.e., seasonal TP increase of 50 cm at each site compared to TP interpolated for 2018 and 2019 summers) predicted that the RI05 site should have ALT and GSS increases of 20.7 and 29.3 cm, respectively (Figure 4). Further, for a 50 cm TP increase, ALT at the RI08 site is expected to increase slightly more (maximum ALT increase of 31.2 cm) than at the RI05 site. In addition, the GS at the RI08 site should subside an additional 18.8 cm if the upper 50 cm of permafrost thaws. Field and laboratory observations showed that both cores hosted an ice-rich zone (Figure 2). Yet, EIC is slightly higher with depth in the RI05 core, translating to a higher predicted GSS and lower ALT increase. Conversely, the ALT increase at the RI07 site followed by thaw penetration increases since almost no excess ice was measured in the upper permafrost section: ALT increased by 44.1 cm, and GS subsided by only 5.9 cm.

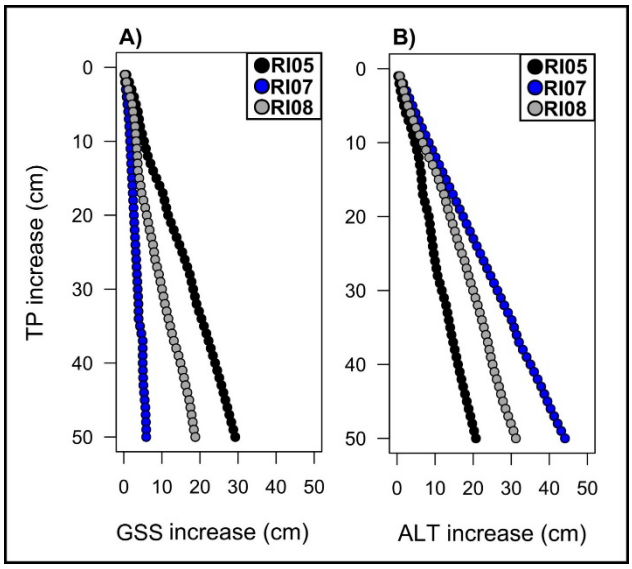

Figure 4. EIC-based GSS and ALT increase predictions in response to TP increases (1 cm increments; maximum of 50 cm) at the three surficial geology sites.

5 Discussion

5.1 Comparing CT and laboratory-derived ground ice content measurements

CT scan-derived VIC estimates (VIC-CT) mostly underapproximated laboratory-derived VIC (VIC-Lab) measurements (Figure 5). Linear regression analyses (with and without including organic-rich sections) revealed moderate correlations between VIC-CT and VIC-Lab for the RI05 and RI08 cores. Conversely, VIC-CT and VIC-Lab were poorly correlated for the RI07 core and sediments in the deeper portion of our RI08 core; VIC-CT in the latter unit was ~0% when measured VIC ranged between ~20 and 40%. Although we do not yet have reliable granulometric data (besides in situ qualitative observations), we suggest that this may have been caused by the coarse pixel resolution of our CT scan images (0.6 mm), making them partially (or completely) spatially unresolvable. This assumption is supported by studies conducted by Calmels et al. (2010) and Lapalme et al. (2017), which demonstrated that CT scans might not spatially resolve pore ice content in sediments if the pixel size is larger than the average pore space. In fact, Lapalme et al. (2017) demonstrated that for permafrost sand-rich sediments, the segmentation of CT scan images may be better suited to estimate EIC, with porosities of ~30–50% and pore-space diameters within the pixel resolution range of CT scan images. Further, for the RI05 core, VIC-CT overestimated VIC-Lab measurements made in its organic-rich section (i.e., the top of the active layer). We hypothesize this is due to the presence of organics having densities similar to water/ice (e.g., Calmels et al., 2010) and, therefore, having been classified as (almost) pure ice during our image segmentation. We suspect this material density issue might also have affected the peat-rich active layer section of the RI08 core but to a lesser extent than the organics in the RI05 core since laboratory measurements confirmed that the former contained larger amounts of VIC.

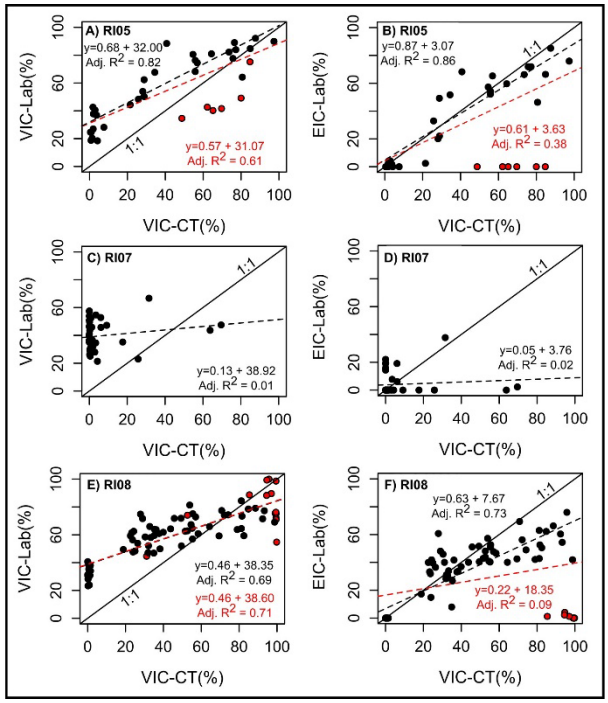

Figure 5. Computed tomography-derived VIC (VIC-CT) averaged over our sampling depth interval (2 cm) compared with laboratory-derived volumetric and EIC (VIC-LAB; EIC-Lab). Red dots indicate measurements made within organic-rich sections of the RI05 and RI08 cores. Measurements made within organic-rich sections were either included (red dotted line and text) or removed (black dotted line and text) from our linear regression analyses.

The comparison of VIC-CT vs. EIC-Lab for our three cores yielded contrasting results. For instance, laboratory analyses of the RI07 core suggest it contained very little or no EIC, yet simultaneously, VIC-CT sometimes overestimated EIC-Lab (Figure 5D). We believe that laboratory manipulation errors may have caused this. This is because the highest VIC-CT values for this core (~64–70% range) were at depths where ice lenses were present (i.e., 170–172 cm), yet our laboratory measurements did not point to high EIC at those depths, suggesting a partial (or complete) omission of those ice-rich segments in our laboratory measurements. Further, when organic-rich core sections were omitted, VIC-CT and EIC-Lab for the RI05 and RI08 cores were moderately linearly correlated. However, including organic-rich sections of those cores for VIC-CT vs. EIC linear regressions led to severe declines in adjusted R^2 values. This is because laboratory measurements indicated that their EIC was nil, while VIC-CT suggested moderate to high (50 to 100%) VIC in the upper organic-rich sections. Still, EIC in the organic-rich sections of the frozen active layer at those two sites may have been higher than we measured in the lab. This is because EIC-Lab measures highly depend on the volume of supernatant waters in respective HDPE tubes once core sections are left to thaw. Accordingly, it is plausible that organics may have absorbed supernatant waters while thawing those frozen active layer core slices.

Overall, our inability to adequately predict VIC or EIC in our cores using CT scan images was likely mostly imputable to the sediments having pore diameters above and below the CT pixel resolution. It is further unclear if this could be attributed to human-induced errors (e.g., difficulties correlating actual depths between CT scan images and laboratory). Nonetheless, what is clear is that our CT scan yields poorly reliable ground ice content estimations when organics are present (i.e., materials having similar densities to water/ice). This supports our decision to rely on laboratory-derived measurements to properly quantify ground ice in our samples to assess the thaw settlement potential of investigated surficial geology units discussed in the following section. Additionally, we plan on alleviating the likely pixel resolution issue by employing a high-resolution X-ray Computed Tomography (HRXCT) approach in the future if we do repeat CT scan analyses on frozen active layer/permafrost samples from this area (e.g., Nitzbon et al. 2022).

5.2 Observed and predicted ground subsidence during the 2018 and 2019 summers

The temporal evolution of observed GSS matched the EIC-based GSS predictions for the RI05 and RI07 sites over the 2018 summer. However, they also show that predicted GSS at the RI08 site lagged what we observed in the 2019 summer (Figure 4). We suggest that the offset between observed and predicted thaw-induced GSS at the RI08 site may have been caused by the behaviour of the 40 cm thick organic-rich (i.e., peat) top layer during the thawing season. Unlike unconsolidated sediments in permafrost, peat may retain its structure upon thawing (especially in poorly drained sites such as RI08; e.g., MacFarlane and Williams 1974). Hence, the collapse of this peat unit may only have been initiated in mid to late-July 2019, once the thaw front reached the underlying unconsolidated mineral soils (and started melting their EIC), as suggested by the observed GSS.

5.3 Active layer thickness deepening and ground surface subsidence under climate warming

Our permafrost degradation simulations enabled us to make site-specific predictions about ALT and GSS dynamics under climate warming. Notably, we showed that soils at our site hosting the least amount of excess ice (RI07) in the near-surface permafrost should not subside that much (~6 cm) under a 50 cm TP increase (i.e., ALT should instead roughly follow TP increases). Accordingly, future ALT measurements at site RI07 could serve as reliable proxies in assessing the magnitude of upper-permafrost thaw. However, this finding does not apply to our two other sites because their near-surface permafrost hosts substantial amounts of excess ice: a 50 cm TP increase and accompanying melting of excess ice at sites RI05 and RI08 should only lead to ALT increases of ~21 and ~32 cm. Ergo, this rudimentary EIC-based modelling demonstrates that ALT and GSS measurements should simultaneously be used to monitor the state of the ground ice in the upper permafrost units of the RI05 and RI08 sites, where EIC is low. This supports findings from previous studies, showing that ALT measurements alone at ice-rich sites may serve as poor permafrost degradation metrics (e.g., Shiklomanov et al. 2013; O'Neil et al. 2023) and that GSS and TP trends are more accurate at characterizing this phenomenon. Hence, care should be taken to pursue the area's ALT and GSS monitoring efforts to properly assess the permafrost's stability under climate change.

In addition, considering that those simulations are based on punctual measurements and site-specific conditions strongly influence ground ice content and distribution, our derived results should be used with prudence for extrapolations to other areas near the hamlet of Rankin Inlet with similar surficial deposits. Upscaling those findings to other areas near Rankin Inlet in hopes of providing first-order estimates on their vulnerability to climate change (e.g., destabilization potential) will most certainly require additional ground ice content measurements (especially concerning EIC) to be repeated within other areas near the hamlet hosting the same surficial units. Then, we will be able to confidently establish the vulnerability of the permafrost in the various surficial geology units occupying this area of Nunavut's Kivalliq region.

6 CONCLUSIONS

Results from the following ground ice content investigation of frozen active layer/permafrost cores taken within the vicinity of Rankin Inlet have led us to the following conclusions:

1) Our field sampling and laboratory results suggest significant excess ice occurs in surficial geology units around Rankin Inlet (NU).

2) Laboratory-derived measurements and CT scan-based estimations of VIC and EIC in our three cores produced conflicting results. We suspect this to be due to a) the low pixel resolution of our CT scan image; b) the presence of materials with similar densities as water/ice (e.g., organics); or c) human-induced errors (e.g., difficulties correlating actual depths between CT scan images and laboratory).

3) Our permafrost degradation scenario demonstrates that subsidence of 5.9 to 29.3 cm can be expected upon thawing of the upper 50 cm of permafrost at the three sites. This quantification of potential thaw effects is helpful for infrastructure development planning.

4) Further efforts will aim to investigate ground ice content (including distribution) and sediment grain size within the various surficial geology units of the Rankin Inlet area/Kivalliq region. This will allow us to make broader predictions concerning the fate of the permafrost in the area under future climate warming.

7 ACKNOWLEDGEMENTS

This work was undertaken via the Climate Change Geoscience and GEM-GeoNorth programs (Natural Resources Canada, contribution number 20210439). Andrew Branson and Kevin Brewer provided field assistance during the 2018 and 2019 field seasons. An internal review by H.B. O'Neil helped improve the paper. We thank the reviewers for their constructive comments.

8 REFERENCES

Calmels, F. and Allard, M. 2004. 'Ice segregation and gas distribution in permafrost using tomodensitometric analysis', *Permafrost and Periglacial Processes* 15, pp. 367–378. Available at: https://doi.org/10.1002/ppp.508.

Calmels, F., Gagnon, O., and Allard, M. 2005. 'A portable earth-drill system for permafrost studies', *Permafrost and Periglacial Processes*, 16, pp. 311–315. Available at: https://doi.org/10.1002/ppp.529.

Calmels, F. and Allard, M. 2008. 'Segregated ice structures in various heaved permafrost landforms through CT Scan', *Earth Surface Processes and Landforms* 33, pp. 209–225. Available at: https://doi.org/10.1002/esp.1538.

Calmels, F., Clavano, W.R., and Froese, D.G. 2010. 'Progress on X-ray computed tomography (CT) scanning in permafrost studies', in *Geo2010: 63rd Canadian Geotechnical Conference*. Calgary, Alberta, Canada.

Castagner, A., Brenning, A., Gruber, S., and Kokelj, S.V. 2022. 'Vertical distribution of excess ice in icy sediments and its statistical estimation from geotechnical data (Tuktoyaktuk Coastlands and Anderson Plain, Northwest Territories)', *Arctic Science* 9(2), pp. 483–496. Available at: https://doi.org/10.1139/as-2021-0041.

Crory, F.E. 1973. 'Settlement associated with the thawing of permafrost', in *2nd International Conference on Permafrost*. Yakutsk, U.S.S.R.: North American Contribution, pp. 599–607.

Doré, G., Niu, F., and Brooks, H. 2016. 'Adaptation methods for transportation infrastructure built on degrading permafrost', *Permafrost and Periglacial Processes* 27(4), pp. 352–364. Available at: https://doi.org/10.1002/ppp.1919.

Dyke, A.S. 2004. 'An outline of North American deglaciation with emphasis on central and northern Canada', *Developments in Quaternary Sciences* 2, pp. 373–424. Available at: https://doi.org/10.1016/S1571-0866(04)80209-4.

Environment and Climate Change Canada (2022). 'Historical climate data', *Environment and Climate Change Canada*. Available at: climate.weather.gc.ca (Accessed: January 2022).

Fan, X.W., Lin, Z.J., Gao, Z.Y., et al. 2021. 'Cryostructures and ground ice content in ice-rich permafrost area of the Qinghai-Tibet Plateau with Computed Tomography Scanning', *Journal of Mountain Science* 18(5). Available at: https://doi.org/10.1007/s11629-020-6197-x.

French, H.M. 2017. *The Periglacial Environment*. United Kingdom: Wiley.

Gadylyaev, D., Nitzbon, J., Schlüter, S., Köhne, J.M., Grosse, G., and Boike, J. 2021. 'Applying Computed Tomography (CT) scanning for segmentation of permafrost constituents in drill cores', *EGU General Assembly 2021*, online, 19–30 Apr 2021, EGU21-11395. Available at: https://doi.org/10.5194/egusphere-egu21-11395.

Golder Associates Ltd. 2014. 'SD 6-1 permafrost thermal regime baseline studies – Meliadine Gold Project', unpublished report for *Agnico-Eagle Mines Limited*. Golder Doc 225-1314280007 Ver. 0. Available at: https://www.nirb.ca/application?strP=r.

Golder Associates Ltd. 2021. 'Meliadine Extension – 2020 Thermal Assessment – Meliadine Gold Project', unpublished report prepared for *Agnico-Eagle Mines Limited*, Golder Doc 20136436-815-R-Rev2-2200. Available at: https://www.nirb.ca/application?strP=r.

Kokelj, S.V. and Burn, C.R. 2003. 'Ground ice and soluble cations in near-surface permafrost, Inuvik, Northwest Territories Canada', *Permafrost and Periglacial Processes* 14, pp. 275–289. Available at: https://doi.org/10.1002/ppp.458.

Lapalme, C.M., Lacelle, D., Pollard, W., Fortier, D., Davila, A., McKay, C.P. 2017. 'Cryostratigraphy and the sublimation unconformity in permafrost from an ultraxerous environment, University Valley, McMurdo Dry Valleys of Antarctica', *Permafrost and Periglacial Processes* 28(4), pp. 649–662. doi:10.1002/ppp.1948.

Lawley, C.J M., McNicoll, V., Sandeman, H., Pehrsson, S., Simard, M., Castonguay, S., Mercier- Langevin, P., and Dubé, B. 2016. 'Age and geological setting of the Rankin Inlet greenstone belt and its relationship to the gold endowment of the Meliadine gold district, Nunavut, Canada', *Precambrian Research* 275, pp. 471–495. Available at: https://doi.org/10.1016/j.precamres.2016.01.008.

LeBlanc A.-M., Oldenborger G.A., and Short, N. 2019. 'Mapping permafrost and terrain conditions by combining corrected DInSAR seasonal and inter-annual ground displacements', *Cold Regions Engineering 2019*, pp. 616–624.

LeBlanc, A.-M. and Oldenborger, G.A. 2021. 'Ground temperature, active-layer thickness and ground-ice conditions in the vicinity of Rankin Inlet, Nunavut', in *Canada-Nunavut Geoscience Office* Summary of Activities 2020, pp. 63–72.

McCuaig, S., McKillop, R., McGregor, C., Roy-Leveillée, P., and St-Amour, A. 2022. 'Mapping and Investigating Permafrost along the Proposed Kivalliq Hydro-Fibre Link, Manitoba to Nunavut', *GeoCalgary 2022*. Calgary, Alberta, Canada: October 2–5, 2022.

MacFarlane, I.C. and Williams, G.P. 1974. 'Some Engineering Aspects of Peat Soils', in *A.R. Aandahl (ed.) Histosols: Their Characteristics, Classification, and Use*, volume 6. Available at: https://doi.org/10.2136/sssaspecpub6.c7.

McMartin, I. 2002. 'Surficial geology, Rankin Inlet, Nunavut', *Geological Survey of Canada* Open File 4116, scale 1:50 000.

McMartin, I., Gauthier, M., and Page, A. 2023. 'Updating the limits of the postglacial marine transgression along western Hudson Bay in mainland Nunavut and northern Manitoba, Canada', in *INQUA 2023 Congress*. Rome, Italy: July 14–20, 2023.

Oldenborger, G.A., Bellehumeur-Génier, O., Short, N., Tremblay, T., and LeBlanc, A.-M. 2017. 'Ground temperatures and permafrost conditions, Rankin Inlet, southern Nunavut', in *Canada-Nunavut Geoscience Office* Summary of Activities 2017, pp. 117–128.

Oldenborger, G.A., Short, N., and LeBlanc, A.-M. 2020. 'Electrical conductivity and ground displacement in permafrost terrain', *Journal of Applied Geophysics* 181, 104148. Available at: https://doi.org/10.1016/j.jappgeo.2020.104148.

O'Neil, H.B., Smith, S.L., Burn, C.R., Duchesne, C., and Zhang, Y. 2023. 'Widespread Permafrost Degradation and Thaw Subsidence in Northwest Canada', *Journal of Geophysical Research: Earth Surface* 128(8), e2023JF007262. Available at: https://doi.org/10.1029/2023JF007262.

Nitzbon, J., Gadylyaev, D., Schlüter, S., Köhne, J.M., Grosse, G., and Boike, J. 2022. 'Brief communication: Unravelling the composition and microstructure of a permafrost core using X-ray computed tomography', *The Cryosphere* 16, pp. 3507–3515. Available at: https://doi.org/10.5194/tc-16-3507-2022.

Pullman, E.R., Jorgenson, M.T., and Shur, Y. 2007. 'Thaw Settlement in Soils of the Arctic Coastal Plain, Alaska', *Arctic, Antarctic, and Alpine Research* 39(3), pp. 468–476. Available at: https://doi.org/10.1657/1523-0430(05-045)[PULLMAN]2.0.CO;2.

Randour, I., McMartin, I., and Roy, M. 2016. 'Study of the postglacial marine limit between Wager Bay and Chesterfield Inlet, western Hudson Bay, Nunavut', in *Canada-Nunavut Geoscience Office* Summary of Activities 2016, pp. 51–60.

R Core Team 2023. 'R: A language and environment for statistical computing', *R Foundation for Statistical Computing*. Vienna, Austria. Available at: https://www.R-project.org/.

Riseborough, D. 2008. 'Estimating active layer and talik thickness from temperature data: implication for modeling results', in D.L. Kane and K.M. Hinkel (eds.), *Proceedings of the Ninth International Conference on Permafrost*. Fairbanks, Alaska, United States: June 29–July 3, 2008, v. 2, pp. 1487–1492.

Shiklomanov, N.I., Streletskiy, D.A., Little, J.D., and Nelson, F.E. 2013. 'Isotropic thaw subsidence in undisturbed permafrost landscapes', *Geophysical Research Letters* 40, pp. 6356–6361, doi:10.1002/2013GL058295.

Watson, G., Slusarchuk, W., and Rowley, R. 1973. 'Determination of Some Frozen and Thawed Properties of Permafrost Soils', *Canadian Geotechnical Journal* 10, pp. 592–606. Available at: https://doi.org/10.1139/t73-055.

Taber, S. 1930. 'The Mechanics of Frost Heaving', *The Journal of Geology* 38, pp. 303–317. Available at: https://doi.org/10.1086/623720.

van Everdingen, R.O. 2005. 'Multi-language glossary of permafrost and related ground-ice terms', *International Permafrost Association*. Available at: http://globalcryospherewatch.org/reference/glossary_docs/Glossary_of_Permafrost_and_Ground-Ice_IPA_2005.pdf (Accessed: 13 Aug 2020).